JOURNAL OF AIRCRAFT
Vol. 37, No. 5, September–October 2000

Optimization of Flexible Wing Without Ailerons for Rolling Maneuver

N. S. Khot*
U.S. Air Force Research Laboratory, Wright–Patterson Air Force Base, Ohio 45433
K. Appa†
Northrop Grumman Corporation, El Segundo, California 90245
and
F. E. Eastep‡
University of Dayton, Dayton, Ohio 45469

An optimum flexible wing structure with enhanced roll maneuver capability at high dynamic pressures is designed. A flexible wing optimized for weight with constraints on strength for 9-*g* symmetric pull-up maneuver at $M = 0.85$ and constraints on the frequency distribution were used. Elastic twist and camber are achieved by providing a system of actuating elements distributed within the internal substructure of the wing to provide control forces. The modal approach was used to develop equilibrium equations for the steady roll maneuver of a wing subjected to aerodynamic loads and actuating forces. The distribution of actuating forces to achieve a specified flexible roll rate was determined by using an optimal control design approach. Here, a full-scale realistic wing was considered for the assessment of strain energy as a measure of the necessary power required to produce the antisymmetric twist and camber deformation to achieve the required roll performance.

Nomenclature

A	=	aerodynamic stiffness matrix
$\underline{A}$	=	plant matrix
B	=	input matrix
C	=	matrix relating generalized elastic displacements and actuator forces
F	=	actuator load distribution matrix
H	=	Hamiltonian function
K	=	structural stiffness matrix
M	=	Mach number
p	=	roll rate
p_t	=	required flexible roll rate
Q	=	state weighting matrix
q	=	dynamic pressure
R	=	control weighting matrix
T	=	transformation matrix
α	=	vector of angle of attack
ε	=	error function
η	=	generalized displacements
η_e	=	generalized elastic displacements
λ	=	Langrange multiplier
Φ	=	roll rate
ψ_e	=	flexible modes
ψ_r	=	rigid-body modes

Introduction

THE objective in the multidisciplinary design optimization approach applicable to aircraft structures is to obtain an optimum design satisfying performance requirements from various disciplines such as materials, structures, fluids, controls, etc. The objective function to be minimized may be the weight of the structure or cost, depending on the available information from the system or some performance index. Because of the advancements in computational power available with present-day computers and anticipated future developments, it has become possible to consider more than one performance requirement simultaneously from different disciplines in the design process. This approach of integrating different disciplines in the design approach has many advantages and disadvantages. The advantage is that the final designs would be obtained by proper tradeoff between design requirements from various disciplines. The disadvantage of considering too many design requirements simultaneously is that it makes the design problem too complicated and not feasible for solution due to the capability and performance of presently available optimization programs, hardware, and software.

At present, software is not available that is capable of simultaneously considering all of the design requirements from different disciplines connected with aircraft design and obtaining optimum design in an integrated fashion. This leads to the design process first consisting of a combination of optimizations based on important design requirements and then using this design as a basis for modifications to satisfy other design or performance requirements from other disciplines. This multiple-step design approach may be necessary to satisfy global and local requirements from different disciplines.

The approach selected here is a two-step process. In the first step, optimum design satisfying requirements on strength and frequency distribution are obtained. The optimization problem was solved by using ASTROS version 20 for the design condition of a 9-*g* symmetric pull-up maneuver at $M = 0.85$. The control system is next designed to retwist and recamber the optimum wing to achieve the target flexible roll rate.

Traditionally, a pilot provides a rolling maneuver for the turning of an aircraft with an aileron system by rotation of trailing-edge control surfaces on the right and left wings in a differential sense. The aileron system increases the lift on one wing and decreases lift on the other wing, resulting in a rolling moment producing the rolling maneuver. This is an effective technique for the generation of a rolling moment for an aircraft operating in a low dynamic pressure environment where the wings are essentially rigid. However, if

Presented as Paper 98-4886 at the AIAA/USAF/NASA/ISSMO 7th Symposium on Multidisciplinary Analysis and Optimization, St. Louis, MO, 2–4 September 1998; received 17 February 1999; revision received 18 December 1999; accepted for publication 23 December 1999.

*Senior Research Aerospace Engineer, Structures Division, Air Vehicles Directorate, VASD. Associate Fellow AIAA.
†Principal Engineer, Military Aircraft Division. Associate Fellow AIAA.
‡Professor of Aerospace Engineering, Department of Mechanical and Aerospace Engineering. Associate Fellow AIAA.

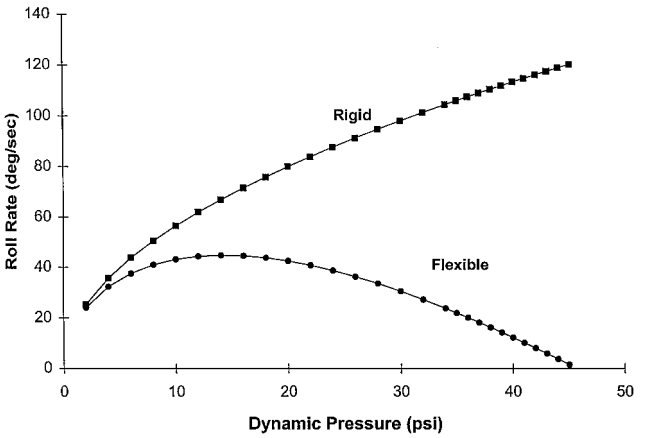

Fig. 1 Loss of roll rate due to wing flexibility.

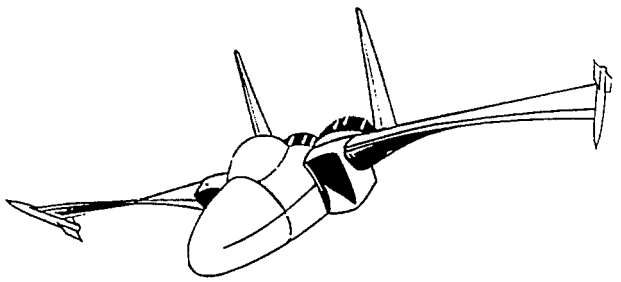

Fig. 2 Rolling aircraft with twisted wings.

the aircraft is operating at high dynamic pressures where the deformation of the wing is significant, the roll rate is reduced (as shown in Fig. 1) by a detrimental aerodynamic twisting moment resulting from the trailing-edge control surface rotation. A roll reversal dynamic pressure, at which the aileron is rendered completely ineffective for producing rolling moment, is also shown in Fig. 1.

Previous investigations[1,2] described a technique for prescribing an elastic wing twist and camber distribution for the enhancement of the rolling maneuver of a wing at all dynamic pressures, with and without ailerons. The control forces were obtained from a technique referred to as fictitious control surfaces. Rather than using an aileron system to achieve an aerodynamic rolling moment, wing deformation is used as an asset rather than an impediment, avoiding the detrimental twisting moment of the aileron and enhancing the roll performance at all dynamic pressures. The wing is twisted and cambered in a differential sense on the right and left sides as shown in Fig. 2 to achieve the required rolling moment for a specified steady roll rate.

One of the main elements of the flexible-wing concept is rolling moment control achieved by the elastic wing twist and camber. This has been investigated previously with an internal actuation scheme,[3,4] multiple external aerodynamic control surfaces,[5,6] and strain-actuated adaptive wings.[7,8] The internal actuation scheme of the mission adaptive wing[3] did achieve aerodynamic benefits through contoured control surface deformation, but the complexity and weight penalty of the actuation system rendered the design impractical. The active flexible-wing technique[5,6] using multiple control surfaces does achieve the proper elastic wing twist for the required rolling moment and results in a decrease of structural weight by relaxing wing stiffness requirements; however, the potential for an aerodynamic penalty exits. Recent developments in smart materials for controlling aircraft structural deformation make it possible to achieve the proper elastic wing twist for control of roll as suggested in Ref. 7, but large actuation strains are required for aeroelastic control of realistic wings.

The Defense Advanced Research Projects Agency has sponsored projects[9] for demonstration of the application of smart materials for twist control to improve aircraft performance based solely on test results from small wind-tunnel models. Technology demonstration based on wind-tunnel model results will result in scale-up issues related to implanting smart wing technologies on an operational aircraft. It is proposed here that a full-scale finite element model of a realistic wing be considered for proper elastic wing twist and camber for roll control in a high dynamic pressure environment. In this investigation, axial load carrying cross rod elements mounted to the internal structure were used as actuators exerting tensile/compressive loads to twist and camber the wing to achieve specified roll rates. In this way, assessments can be made between the energy requirements for twist and camber control to achieve the required roll performance at different dynamic pressures.

Approach

The equilibrium equations for a steady roll maneuver can be written as[10]

$$[K]\{x\} + q[T]^T[A]\{\alpha\} + [F]\{u\} = 0 \tag{1}$$

where $[K]$ is the structural stiffness matrix of the finite element model, $\{x\}$ is the vector of nodal displacement vector, q is the dynamic pressure, $[T]$ is the transformation matrix from the structural degrees of freedom to the aerodynamic degrees of freedom, $[A]$ is the aerodynamic stiffness matrix, $\{\alpha\}$ is the vector for the angle of attack at the aerodynamic panels, $[F]$ is the applied actuator load distribution matrix, and $\{u\}$ is the vector for the actuator stimuli. The product $[F]\{u\}$ is the vector of control forces generated at the structural node points due to the actuator forces $\{u\}$ or due to the voltages applied to the solid-state actuators. In the latter case, the elements of matrix $[F]$ would depend on the number of stacks, number of cycles, and the properties of the solid-state actuators in addition to the direction cosines associated with the actuators.

The displacement vector $\{x\}$ can be defined as a linear combination of rigid-body modes and vibration modes as

$$\{x\} = [\Psi_r]\{\eta_r\} + [\Psi_e]\{\eta_e\} = [\psi]\{\eta\} \tag{2}$$

where $[\Psi_r]$ is the rigid-body mode, $[\psi_e]$ is the specified number of antisymmetric low-frequency modes, and $\{\eta_r\}$ is the generalized rigid-body displacements, equal in the present case to the roll angle ϕ. In Eq. (2), $\{\eta_e\}$ represent the elastic displacements. The subscripts r and e are used to indicate rigid-body and flexible vibration modes, respectively.

The angle of attack $\{\alpha\}$ at the control points of the aerodynamic panels can be written as

$$\{\alpha\} = (1/V)[T]\{\dot{x}\} \tag{3}$$

where V is the freestream velocity. By the use of Eq. (2), the angle of attack can be written as

$$\{\alpha\} = \frac{1}{V}[T]\left[[\Psi_r]p + U\left[\frac{\partial \psi_e}{\partial \bar{x}}\right]\{\eta_e\}\right] \tag{4}$$

where p is the roll rate $\dot{\phi}$, U is the chordwise component of V in the direction $\bar{x}$, and $[(\partial \psi_e)/(\partial \bar{x})]$ is the matrix of the flexible mode gradient with respect to the $\bar{x}$ coordinate. Equation (4) can be written as

$$\{\alpha\} = \left[\frac{\bar{\Psi}_r}{V}\frac{\partial \bar{\Psi}_e}{\partial \eta_e}\right]\begin{Bmatrix} p \\ \eta_e \end{Bmatrix} = [\bar{\alpha}]\{\eta\} \tag{5}$$

where $\bar{\Psi}_r$ and $\bar{\Psi}_e$ are the rigid and vibration modes expressed in aerodynamic degrees of freedom. Using Eq. (5), the equilibrium equation (1) can be written in terms of generalized coordinates as

$$[\bar{K}]\begin{Bmatrix} p \\ \eta_e \end{Bmatrix} + q[\bar{A}]\begin{Bmatrix} p \\ \eta_e \end{Bmatrix} + [\bar{F}][u] = 0 \tag{6}$$

where

$$[\bar{K}] = \begin{bmatrix} 0 & 0 \\ 0 & [\Psi_e]^T[K][\Psi_e] \end{bmatrix} \tag{7}$$

$$[\bar{A}] = [\Psi]^T[T]^T[A][\bar{\alpha}] \tag{8}$$

$$[\bar{F}] = [\Psi]^T[F] \tag{9}$$

Solving Eq. (6) for the generalized coordinates gives

$$\begin{Bmatrix} p \\ \eta_e \end{Bmatrix} = -[[\bar{K}] + q[\bar{A}]]^{-1}[\bar{F}]\{u\} \tag{10}$$

or

$$\begin{Bmatrix} p \\ \eta_e \end{Bmatrix} = \begin{bmatrix} B \\ C \end{bmatrix}\{u\} \tag{11}$$

The roll rate p is given by

$$p = [B]\{u\} \tag{12}$$

and the generalized coordinates of the elastic modes are given by

$$\{\eta_e\} = [C]\{u\} \tag{13}$$

For the specified distribution of actuator forces $\{u\}$, Eq. (13) can be used to calculate the roll rate p. However, for achieving the target roll rate p_t at a specified Mach number and specified dynamic pressure, it was required to use the control design approach to determine the distribution of actuator forces necessary to deform the wing.

The control design algorithm used in this paper is based on the optimal control approach. The linear state equation can be written as

$$\{\dot{\underline{x}}\} = [\underline{A}]\{\underline{x}\} + [B]\{u\} \tag{14}$$

where $\{\underline{x}\}$ is the state vector, $[\underline{A}]$ is the plant matrix, $[B]$ is the input matrix, and $\{u\}$ is the control input vector. The Hamiltonian function can be written as

$$H = \tfrac{1}{2}\{\varepsilon\}^T[Q]\{\varepsilon\} + \tfrac{1}{2}\{u\}^T[R]\{u\} + \{\lambda\}^T[[\underline{A}]\{\underline{x}\} + [B]\{u\}] \tag{15}$$

where $[Q]$ and $[R]$ are the state and control weighting matrices. These matrices must be positive semidefinite and positive definite, respectively. In Eq. (15), $\{\varepsilon\}$ is the vector of the target error function and $\{\lambda\}$ is the vector of the Langrange multipliers. The necessary conditions for optimality can be obtained by differentiating the Hamiltonian function with respect to $\{\underline{x}\}$, $\{u\}$, and $\{\lambda\}$, and are given by

$$\begin{bmatrix} \dot{\underline{x}} \\ \dot{\lambda} \end{bmatrix} = \begin{bmatrix} [\underline{A}] & -[B][R]^{-1}[B]^T \\ -[Q] & -[\underline{A}]^T \end{bmatrix}\begin{bmatrix} \underline{x} \\ \lambda \end{bmatrix} + \begin{bmatrix} 0 \\ [Q]\{r\} \end{bmatrix} \tag{16}$$

$$\{u\} = -[R]^{-1}[B]^T\{\lambda\} \tag{17}$$

where $\{r\}$ is the desired state vector. A solution to Eqs. (16) and (17) would give the desired control vector minimizing the Hamiltonian function.

For the rolling maneuver control problem, Eq. (12) defines the state equation. We have only one state roll rate p and the plant matrix $[\underline{A}]$ has only one element and is equal to -1.0. By the definition of the target roll rate by p_t, the target error function can be written as

$$\varepsilon(1) = (1 - p/p_t) \tag{18}$$

By the use of Eqs. (16) and (18), the optimality conditions for the rolling maneuver control problem are given by

$$\begin{bmatrix} \dot{p} \\ \dot{\lambda} \end{bmatrix} = \begin{bmatrix} h_{11} & h_{12} \\ h_{21} & h_{22} \end{bmatrix}\begin{bmatrix} p \\ \lambda \end{bmatrix} + \begin{bmatrix} 0 \\ F2 \end{bmatrix} \tag{19}$$

where

$$h_{11} = -1.0 \tag{20}$$

$$h_{12} = -[B]R[B]^T \tag{21}$$

$$h_{21} = -\left(Q/p_t^2\right) \tag{22}$$

$$h_{22} = -h_{11} \tag{23}$$

$$F_2 = (Q/p_t) \tag{24}$$

Because in the present problem we are interested only in the steady rolling maneuver, the left side of Eq. (19) can be set to zero, and this gives

$$\begin{bmatrix} p \\ \lambda \end{bmatrix} = -\begin{bmatrix} h_{11} & h_{12} \\ h_{21} & h_{22} \end{bmatrix}^{-1}\begin{bmatrix} 0 \\ F_2 \end{bmatrix} \tag{25}$$

and the actuator input for required roll rate p_t is given by

$$\{u\} = -[R]^{-1}[B]^T\lambda \tag{26}$$

Design of the control system and the evaluation of the generalized displacement vector $\{\eta\}$ corresponding to the desired roll rate p_t was iterative due to the nonlinear nature of the problem. For the specified weighting parameters in the definition of the performance index, the elements of the generalized displacement vector $\{\eta\}$ were assigned initial values. The iteration procedure was continued until the target error function $\varepsilon(1)$ in Eq. (18) was very small. The generalized displacement vector $\{\eta\}$ and control vector $\{u\}$ determined by this procedure satisfied the generalized equilibrium equation (6), and the roll rate was equal to the desired value p_t.

The Unified Subsonic and Supersonic Aerodynamic Analysis (USSAERO)[11] program was used for the computation of aerodynamic loads on the aircraft wing. This approach uses a superposition of vortex singularities applied to a discrete number of aerodynamic panels to calculate the discrete pressure distribution over the wing surface. This algorithm is capable of accounting for the aerodynamic force produced by twist and camber, control surface rotation, and structural deformation by satisfying tangential flow conditions at the control points of each aerodynamic panel.

In this investigation, numerical calculations for rigid and flexible vibration modes, aerodynamic stability derivatives, generalized stiffness matrix, etc., are calculated from ASTROS.[12] The special version of ASTROS was run with bulk data containing the location and description of the actuators. In the present case, the actuators were assumed to be rod elements capable of exerting only axial loads. The required data for solution of the approach discussed in the last section were written on separate files after execution of the ASTROS run and was used to design the actuating system to achieve a specified roll rate at different dynamic pressures.

The strain energy U was found by

$$U = \tfrac{1}{2}\{\eta\}^T[[\bar{K}] + q[\bar{A}]]\{\eta\} \tag{27}$$

which is also equal to the total work done by all of the actuators. The displacements of the structural node points were calculated to study the deformation patterns.

Numerical Examples

A fighter-type wing was selected as representative of a low-aspect-ratio wing. The wing planform is shown in Fig. 3 along with the location of the underlying structure. The aerodynamic paneling for this wing is also shown in Fig. 3. The wing planform as shown in Fig. 3 was divided into 12 sections along the chord and 15 sections along the span, giving a total of 180 aerodynamic boxes. The underlying structure consisting of 10 spars and 6 ribs is represented with finite elements, as shown in Fig. 4. The wing structure was idealized using 133 nodes. Top and bottom skins were idealized with CQUAD4 and CTRIA3 elements. Spar and web caps were idealized with CBAR elements, and webs were idealized with CSHEAR and CROD elements. RBAR elements were used for rigid attachments for extra splining of grid nodes. Only the translational degrees of

freedom were retained associated with the CQUAD4 and CTRIA3 elements. Appropriate single-point and multipoint constraints were specified for proper simulation of the wing structure connection to the fuselage. An 8000-lb mass was used to simulate the weight of the fuselage and a total of 1600 lb of nonstructural mass, which includes weight of fuel, was distributed among different node points on the wing structure.

The flexible-wing structure was designed satisfying stress and frequency constraints using ASTROS[13] version 20. Von Mises stress constraints were imposed for the design condition of a 9-g symmetric pull-up at $M = 0.85$ at the reference pressure of 30 psi. Even though at $M = 0.85$ at sealevel the dynamic pressure is equal to 7.4 psi, a higher value was used to increase the magnitude of the applied load and to achieve aerodynamic distribution instead of a concentrated static or uniformly distributed load. A lower-bound frequency constraint of 3 Hz was specified for the symmetric second mode. The first mode was a rigid mode with zero frequency. The details of the minimum weight design are not given due to length restrictions. The first six frequencies, in hertz, associated with the flexible symmetric modes for the initial and the optimum designs were 6.00, 25.81, 33.72, 40.95, 60.92, and 81.04, and 3.00, 9.46, 14.86, 19.66, 20.01, and 26.42. The frequency constraint specified on the first frequency was nearly satisfied as an equality constraint. The stress distributions in all the elements satisfied the von mises stress criteria, and the optimum design obtained after 40 iterations was a feasible design.

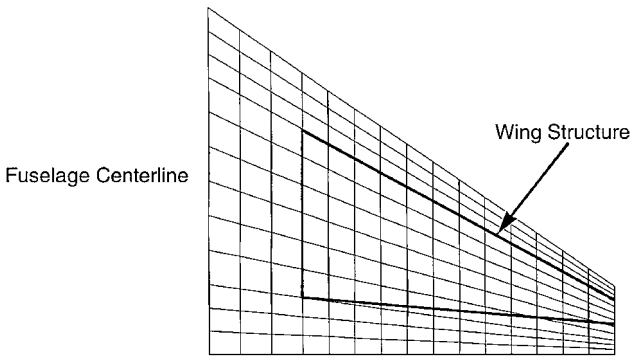

Fig. 3 Aerodynamic grid.

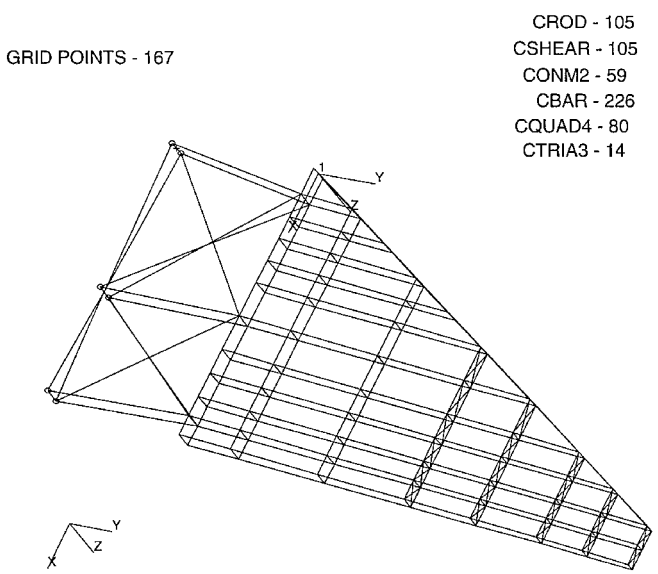

Fig. 4 Finite element model.

The 1 rigid and 15 flexible modes were considered for this study in the definition of the $\{\eta\}$ vector in Eq. (2). Because the rolling maneuver was associated with the antisymmetric vibration modes, the distribution of flexible frequencies was not the same as those given corresponding to symmetric pull-up. The first five frequencies, in hertz, associated with the antisymmetric mode for the optimum design were 5.74, 13.86, 14.92, 19.66, and 23.26, respectively. These values are greater than for the symmetric modes.

The actuating system to twist and camber the wing consisted of 40 cross rods along the five ribs as shown in Fig. 4. Actuators were of a generic nature, capable of providing tensile or compressive forces as required to deform the wing to achieve the specified flexible roll rate. The required total strain energy and the magnitude of forces necessary to twist the wing to achieve specified flexible roll rate at different dynamic pressures were calculated under subsonic and supersonic design conditions. The design study was conducted at different dynamic pressures between $M = 0.85$ and 2.80 at 20,000-ft altitude. The target flexible roll rate was specified as 90 deg/s at all dynamic pressures.

Table 1 gives the total strain energy requirement in foot pounds calculated using Eq. (27) for both subsonic and supersonic design conditions. The work done by the actuators was also calculated for

Table 1 Strain energy requirements to achieve 90-deg/s flexible roll rate[a]

Mach	Pressure, lb/in.^{2}	Velocity, in./s	Strain energy, ft · lb
0.85	3.41	10,577	1975
1.20	6.81	14,932	131
1.40	9.27	17,421	127
1.60	12.11	19,910	98
1.80	15.32	22,399	70
2.00	18.92	24,888	49
2.20	22.89	27,376	36
2.40	27.24	29,865	25
2.60	31.98	32,354	20
2.80	37.09	34,843	14

[a] Altitude 20,000 ft.

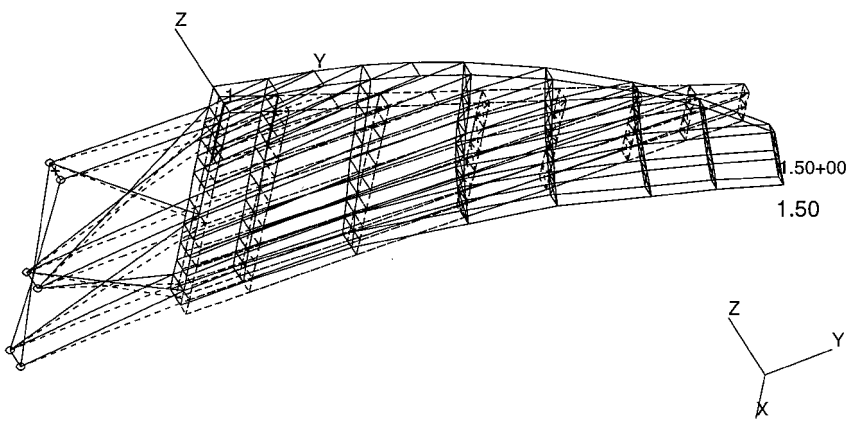

Fig. 5 Wing deformation at M =1.2, flexible roll rate 90 deg/s.

all of the cases and was found to be equal to the strain energy stored in the structural system. The requirement for the strain energy to deform the wing to achieve the roll rate of 90 deg/s decreased with an increase in the Mach number and associated dynamic pressure. The decrease in the energy requirement at high dynamic pressures is due to the increase in the lift pressure helping to create the required rolling moment.

Figures 5 and 6 show the static aeroelastic deformations of the wing required to obtain a flexible roll rate of 90 deg/s at Mach numbers 1.2 and 2.0, respectively. The deformation patterns for both cases are similar, except for the magnitude of deflection at different node points. The maximum deflections at the tip of the trailing edge for $M = 1.2$ and 2.0 were 1.50 and 1.07 in., respectively. The strain energies required for the two cases was 131 and 49 ft · lb, respectively. In both cases the wing bends and twists to provide a positive local angle of attack at all aerodynamic elements. The downward deformation is believed to occur so that full advantage of the geometric coupling between bending and twist due to wing sweep can be utilized to maximize the increase in the local angle of attack of the wing. This deformation pattern and the reduction of

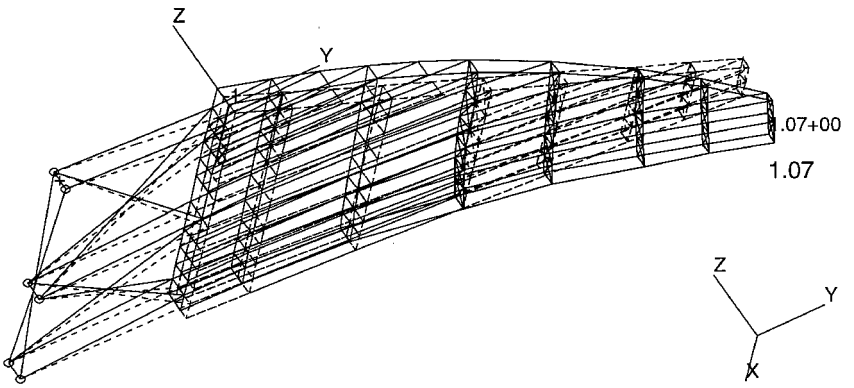

Fig. 6 Wing deformation at $M = 2.0$, flexible roll rate 90 deg/s.

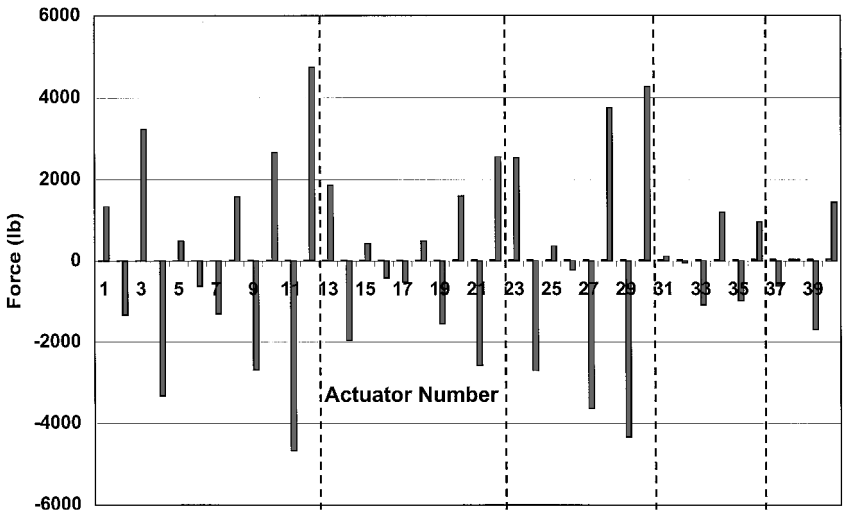

Fig. 7 Actuator force distribution, $M = 1.2$, flexible roll rate 90 deg/s.

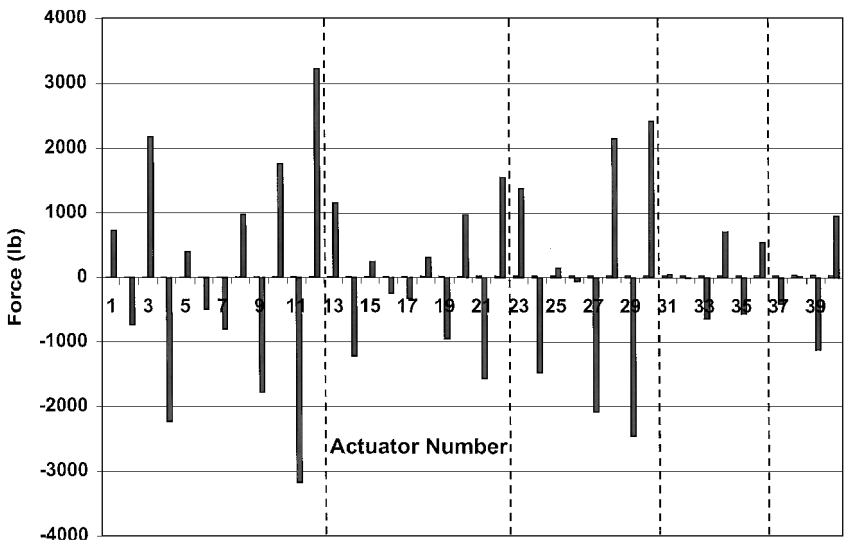

Fig. 8 Actuator force distribution, $M = 2.0$, flexible roll rate 90 deg/s.

the total strain energy at high dynamic pressures indicates that the aeroelastic effects are used to increase the rolling moment.

Figures 7 and 8 show the distribution of forces in the actuators for Mach numbers 1.2 and 2.0, respectively, to achieve a flexible roll rate of 90 deg/s. There were 12, 10, 8, 6, and 4 actuators in five ribs, respectively. The fifth rib was near the tip of the wing and the first rib was farthest from the tip. The actuators were numbered 1–12, 13–22, 23–30, 31–36, and 37–40 in the five ribs starting from the first rib near the fuselage containing the actuators. The numbering in each rib was started from the leading edge of the wing. In Figs. 7 and 8 the vertical dotted lines were drawn to separate the actuators in the five ribs. The magnitude of forces for $M = 1.2$ were larger than those for $M = 2.0$. The maximum forces occurred in both cases in actuators 11 and 12, which were located in the first rib near the trailing edge. The maximum forces were equal to 4604 and 3227 lb for the two Mach numbers 1.2 and 2.0, respectively.

Conclusions

In this investigation, the flexibility of a wing is used as a departure from the traditional aileron system, which results in a detrimental aerodynamic twisting moment and possibly in unacceptable roll performance at high dynamic pressures. A realistic wing was optimized with constraints on the strength and frequency distribution to obtain a feasible flexible wing structure. Rather than using the traditional aileron, we have investigated the use of elastic twist and camber of the whole wing to achieve acceptable roll performance at all dynamic pressures.

A modal-based analytical design approach was used to write the equilibrium equations for a steady roll maneuver, and an optimal control design approach was utilized to determine the distribution of actuator forces. The work done by the actuators was calculated at different Mach numbers and dynamic pressures at an altitude of 20,000 ft to access the energy requirements. The actuating system consisted of rods along the ribs, which were assumed to be of generic nature, capable of exerting tensile or compressive forces as required. At high dynamic pressures the forces in the actuators were of reasonable magnitude. In the near future, it is anticipated that elastic twist, adding camber and providing necessary stiffness to prevent flutter and local buckling, can be achieved through the use of future smart materials and actuating system.

Acknowledgment

The third author acknowledges the support received from the Air Force Office of Scientific Research under the University Residency Research Program during the period of this investigation.

References

[1] Khot, N. S., Eastep, F. E., and Kolonay, R. M., "Method for Enhancement of the Rolling Maneuver of a Flexible Wing," AIAA Paper 96-1391, April 1996.

[2] Khot, N. S., Eastep, F. E., and Kolonay, R. M., "Wing Twist and Camber for the Rolling Maneuver of a Flexible Wing Without Ailerons," AIAA Paper 97-1268, April 1997.

[3] Hall, J. W., "Executive Summary AFTI/F-111 Mission Adaptive Wing," WRDC-TR-89-3083, Sept. 1989.

[4] Austin, F., Knowles, G. J., Jung, W. G., Tung, E. C., and Sheedy, E. M., "Adaptive/Conformed Wing Design for Future Aircraft," 1st European Conf. on Smart Structures and Materials, Glasgow, Scotland, U.K., May 1992.

[5] Miller, G. D., "Active Flexible Wing (AFW) Technology," Air Force Wright Aeronautical Labs., AFWAL-TR-87-3036, Wright–Patterson AFB, OH, Feb. 1988.

[6] Miller, G. D., "Active Flexible Wing Multidisciplinary Design Optimization Method," AIAA Paper 94-4412-CP, Sept. 1994.

[7] Lazarus, K. B., Crawley, E. F., and Bohlmann, J. D., "Static Aeroelastic Control Using Strain Actuated Adaptive Structures," 1st Joint U.S./Japan Conf. on Adaptive Structures, Maui, HI, Nov. 1990.

[8] Beauchamp, C. H., Nadolink, R. H., Dickinson, S. C., and Dean, L. M., "Shape Memory Alloy Adjustable Camber (SMAAC) Control Surfaces," 1st European Conf. on Smart Structures and Materials, Glasgow, Scotland, U.K., May 1992.

[9] Kudva, J., Appa, K., Martin, C., Sendeckyj, G., and Harris, T., "Design, Fabrication, and Testing of the DARPA/WL Smart Wing Wind-Tunnel Model," AIAA Paper, 97-1198, April 1997.

[10] Appa, K., Ausman, J., and Khot, N. S., "Feasibility Assessment and Optimization Study of Smart Actuation Systems for Enhanced Aircraft Maneuver Performance," WL-TR-97-3083, Wright–Patterson AFB, OH, July 1997.

[11] Woodward, F. A., "An Improved Method for the Aerodynamic Analysis of Wing–Body–Tail Configurations in Subsonic and Supersonic Flow, Part I—Theory and Application," NASA CR-2228, Vol. 1, May 1973.

[12] Neill, D. J., and Herendeen, D. L., "Automated Structural Optimization System (ASTROS)" Vol. 1 Users Manual, Air Force Wright Aeronautical Labs., AFWAL-TR-93-3025, Wright–Patterson AFB, OH, March 1993.

[13] *ASTROS User's Reference Manual for Version 20*, Universal Analytics Inc., Torrance, CA, 1997.